Article ID: 1000-324X(2014)04-0443-06 **DOI:** 10.3724/SP.J.1077.2014.13672

Preparation of $LiMn_{0.4}Fe_{0.6}PO_4$/C Composite by A New Route Combining Solid-state Reaction with Hydrothermal Synthesis

LI Jian[1, 2, 3], YAO Shu-Heng[1], ZHOU Hong-Ming[1, 2, 3], GENG Wen-Jun[1]

(1. School of Materials Science and Engineering, Central South University, Changsha 410083, China; 2. Hunan Zhengyuan Institute for Energy Storage Materials and Devices, Changsha 410083, China; 3. Key Laboratory of Nonferrous Metal Materials Science and Engineering of Ministry of Education, Central South University, Changsha 410083, China)

Abstract: The olivine type $LiMn_{0.4}Fe_{0.6}PO_4$ was synthesized *via* a new route that combining solid-state reaction with hydrothermal synthesis from Li_2CO_3, $FeC_2O_4{\cdot}2H_2O$, $MnCO_3$ and $NH_4H_2PO_4$ (at molar ratio of 5:6:4:10). The structure, particle size and surface morphology of these cathode active materials were investigated by XRD, SEM and TEM techniques. The electrochemical properties of $LiMn_{0.4}Fe_{0.6}PO_4$/C as cathode in lithium-ion cells were tested *via* cyclic voltammetry and galvanostatic charge-discharge measurements. Phase-pure particles of size ~120 nm are prepared with a conductive, thin web of carbon surrounding them. Cyclic voltammetry shows the active voltage range of the material which consists of two pairs of redox peaks: 3.5 V corresponding to Fe^{3+}/Fe^{2+} reaction and 4.0 V corresponding to Mn^{3+}/Mn^{2+} reaction. An initial discharge capacity of 160 mAh/g at 0.1*C*, 143 mAh/g and a stable cycling property at 0.5*C* are obtained for the $LiMn_{0.4}Fe_{0.6}PO_4$/C composite.

Key words: Li-ion battery; solid-state reaction; hydrothermal synthesis; electrochemical property; electron microscopy

In recent years, lithium-ion battery have developed rapidly due to the increased market demand for portable electronics, transportation and energy storage. Among the families of cathode materials, $LiFePO_4$ is considered to be one of the most promising candidates for high-power batteries. Many efforts have been made over the past few years to improve the power performance of $LiFePO_4$ by reducing particle size and improving the conductivity of the solid phase[1-8]. High-performance $LiFePO_4$ has appeared now in the field of commercial power Li-ion battery[9].

Since the success of $LiFePO_4$, $LiMnPO_4$ with the same structure and theoretical capacity (170 mAh/g) also receives extensive attention as attractive cathode material. $LiMnPO_4$ has a redox potential of 4.1 V *vs* Li^+/Li, is compatible with existing electrolytic liquid system[10-11]. The voltage platform of 4.1 V *vs* Li^+/Li makes $LiMnPO_4$ has a higher theoretical energy density and lower energy costs than $LiFePO_4$. However, along with low ionic conductivity, the electronic conductivity of $LiMnP_{0.4}$ ($<10^{-10}$ s/cm) is much lower than that of $LiFePo_4$ (1.8×10^{-9} s/cm) causing it difficult to obtain decent electrochemical activity[12-14]. Furthermore, electrochemical performance of $LiMnPO_4$ becomes worse due to Jahn-Teller effect in Mn^{3+} and interface strain owing to mutual transformation between $LiMnPO_4$ and $MnPO_4$ during cycling[15]. So, $LiMnPO_4$ materials with capacities more than 120 mAh/g are rarely attained in contrast to $LiFePO_4$[14-16]. But higher discharge capacity could be attained when Fe and Mn coexist at the octahedral 4c site in the olivine structure. Therefore, $LiMn_yFe_{1-y}PO_4$ has received greater attention in recent years compared with $LiMnPO_4$[10, 16-28].

Among the different synthesis methods, solid-state reaction[16–21] and Sol-Gel method[23] have been widely adopted for preparing carbon-coated $LiMn_yFe_{1-y}PO_4$. However, $LiMn_yFe_{1-y}PO_4$ samples synthesized by conventional solid-state reaction have large micron-sized particles and decreased capacity at higher Mn/Fe ratios. Literatures[18-19, 21] show that the initial discharge capacity at 0.1*C* rate for $LiMn_{0.4}Fe_{0.6}PO_4$/C prepared by the traditional solid phase method is about 145 mAh/g. The particle size can be reduced by low sintering temperature, but it will lead to low crystallinity of material. Low temperature solid-state reaction and hydrothermal synthesis could be co-adopted to prepare uniform $LiMn_yFe_{1-y}PO_4$ particles with small size. The raw materials were decomposed and reacted with each other to form olivine crystal nucleus during the low temperature solid-state reaction, and the

Received date: 2013-12-19; **Modified date:** 2014-01-08; **Published online:** 2014-01-28
Foundation item: Hunan Science and Technology Project(2013GK3002); Changsha Science and Technology Project (K1202039-11)
Biography: LI Jian(1969–), male, PhD. E-mail: ziliao2000@126.com
Corresponding author: ZHOU Hong-Ming, PhD. E-mail: ipezhm@163.com

uniform high-pressure low-temperature environment suppressed the growth of $LiMn_{0.4}Fe_{0.6}PO_4$ particles during the hydrothermal synthesis process. To the best of our knowledge, very few literatures reported in this regard. In this work, we chose the *y* value of 0.4 and develop a new synthesis route for $LiMn_{0.4}Fe_{0.6}PO_4$/C composites by the low temperature solid-state reaction combined with hydrothermal synthesis. We report the details of this new synthesis method of carbon-coated $LiMn_{0.4}Fe_{0.6}PO_4$ samples and their impressive cathode performance.

1 Experimental

1.1 Synthesis of $LiMn_{0.4}Fe_{0.6}PO_4$/C

The carbon-coated $LiMn_{0.4}Fe_{0.6}PO_4$ composite was synthesized by the low temperature solid-state reaction combined with hydrothermal synthesis from the precursors Li_2CO_3, $FeC_2O_4{\cdot}2H_2O$, $MnCO_3$ and $NH_4H_2PO_4$. The method essentially consisted of: (i) blending of all ingredients together in alcohol, then ball milling of the powder at room temperature for 8 h; (ii) drying to get a fine solid powder, then thermal treatment at 400 ℃ and 500 ℃ for 4 h in argon gas atmosphere, respectively; (iii) heating the powder at 180 ℃ for 24 h in a Teflon-lined stainless steel autoclave; (iv) then drying the materials and further sintering at 700 ℃ for 3 h in argon gas atmosphere. About 18wt% of sugar was added along with other ingredients for getting a conductive coating. According to different thermal temperatures, the final products were labeled as T-400 and T-500, respectively.

1.2 Physical characterization

Thermal analysis of the precursor was investigated on a METTLER TOLEDO TGA/SDTA851e apparatus in the temperature range from 25 ℃ to 900 ℃ in flowing nitrogen at a heating rate of 10 ℃/min. The crystallographic structures of the synthesized samples were analyzed by X-ray powder diffraction on a Rigaku-D/ MAX-2500VB diffractometer with Cu Kα radiation (λ=0.15406 nm). Scanning electron microscopy (SEM) imaging was carried by using field-emission scanning microscope (FE-SEM, Sirion 200). The nature of carbon coating was observed with high-resolution transmission electron microscope (HR-TEM, HEM–2100F/UHR).

1.3 Electrochemical evaluation

The working electrode was prepared by mixing the active material, conductive material (Super-P carbon black, Alfa) and binder (PVDF, Aldrich) in the weight ratio of 80:10:10. The viscous slurry of N-methylpyrrolidone (NMP) was then cast on the aluminum foil and dried at 100 ℃ in vacuum for 12 h. The film was cut into circular discs with area of 1.53 cm^2 and mass of 3.2 mg for using as cathode.

The coin type $LiMn_{0.4}Fe_{0.6}PO_4$/Li cell was assembled with lithium metal as anode, Celgard®-2200 as diaphragm and 1 mol/L $LiPF_6$ in ethylene carbonate (EC) /dimethyl carbonate (DMC) (1:1 by volume) as liquid electrolyte. Cyclic voltammetry (CV) was carried out between 2.5 V and 4.5 V to ensure both Fe and Mn redox reactions could take place. Electrochemical performance tests of $LiMn_{0.4}Fe_{0.6}PO_4$/Li cells were evaluated between 2.5 V and 4.5 V *vs* Li/Li^+ at 0.1*C* and 0.5*C* current using an automatic galvanostatic charge-discharge unit at room temperature.

2 Results and discussion

Figure 1(a) and (b) show the XRD patterns for mixtures of raw materials sintered at different temperatures. At 400 ℃ as shown in Fig. 1(a), $LiMPO_4$ (M=Fe, Mn) becomes the dominant phase, but two small impurity peaks marked with the red arrow still exist, corresponding to $Li_4(P_2O_7)$ and $Mn_2P_2O_7$, respectively. As the sintering temperature is increased to 500 ℃, single-phase $LiMn_{0.4}Fe_{0.6}PO_4$ particles are obtained as shown in Fig. 1(b). After sintered at 400 ℃ for 4 h, the mixture was then heated at 180 ℃ for 24 h in purified water, and Fig. 1(c) is its XRD pattern. It shows that two small impurity peaks disappear and single-phase $LiMn_{0.4}Fe_{0.6}PO_4$ particles are obtained with well-defined olivine structure (orthorhombic Pnma). The reason of disappearance of the impurity peaks has yet to be in-depth study.

The TG/DTA measurement of the starting materials composed of Li_2CO_3, $FeC_2O_4{\cdot}2H_2O$, $MnCO_3$ and $NH_4H_2PO_4$ is presented in Fig. 2. Two endothermic peaks at 180 ℃ and 230 ℃ in the DTA curve are observed, corresponding to the decomposition of $NH_4H_2PO_4$ and

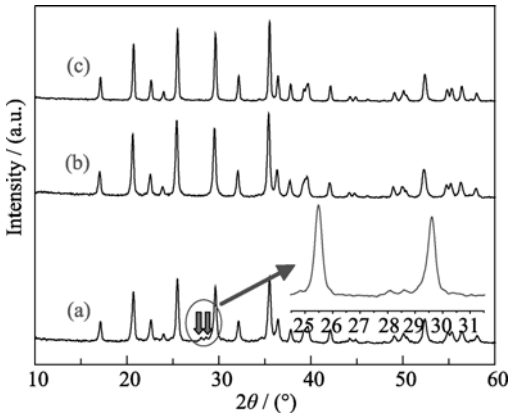

Fig. 1 XRD patterns for a mixture of raw materials sintered at 400 ℃ for 4 h (a), at 500 ℃ for 4 h (b) and at 400 ℃ for 4 h, and then heated at 180 ℃ for 24 h in distilled water (c)

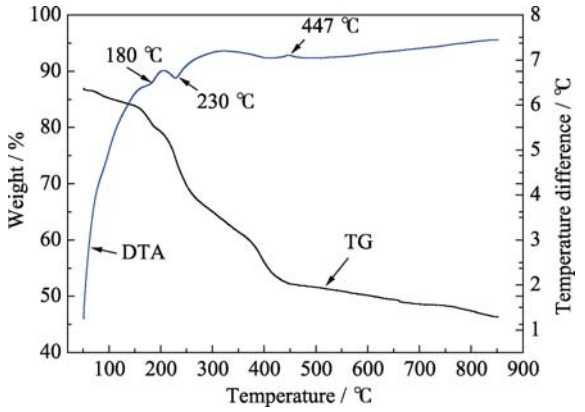

Fig. 2 TG and DTA curves of the precursors synthesized from Li_2CO_3, $FeC_2O_4{\cdot}2H_2O$, $MnCO_3$ and $NH_4H_2PO_4$ (5:6:4:10 in mole)

losing lattice water of $FeC_2O_4{\cdot}2H_2O$, respectively[29]. No other endothermic peaks are found in DTA curves under 445 ℃, but continual weight loss is observed in TG curve. The weight loss under 445 ℃ is about 47.5%. It indicates that FeC_2O_4 should be decomposed and reacted with the decomposed product of $NH_4H_2PO_4$. From 230 ℃ to 500 ℃, an exothermic peak appears between 230 ℃ and 425 ℃, implying the formation of $LiFePO_4$ as confirmed by XRD data. Another exothermic peak at 445 ℃ can be ascribed to crystallization of the amorphous $LiMPO_4$[30].

The morphology of samples was further examined by SEM. Figure 3 shows SEM images of $LiMn_{0.4}Fe_{0.6}PO_4$/C synthesized by the new route. It can be easily seen that the temperature of solid-state reaction has a significant influence on the morphology of the final prepared samples. The particles of T-400 prepared at 400 ℃ are homogeneous with the particle size of about 120 nm. When the temperature is changed to 500 ℃, the primary particle size of T-500 becomes bigger and falls into the range of 120–500 nm, which is much larger than that of T-400.

The TEM and SAED were applied to further investigate the microstructure and confirm the carbon distribution and crystallinity of the prepared samples. Figure 4 shows the TEM image and SAED pattern of T-400. As shown in Fig. 4(a), the surface of core $LiMn_{0.4}Fe_{0.6}PO_4$ is wrapped with a thin film, which is favorable to the electronic connection of the inter-particles. In addition, the high-resolution TEM (HRTEM) image (Fig. 4(b)) demonstrates that the coating is about 10 nm in thickness. And there are no lattice fringes on the surface of $LiMn_{0.4}Fe_{0.6}PO_4$, indicating that the surface carbon is in an amorphous state. The related SAED (Fig. 4(c)) pattern indicates that the core particle is single-crystalline and can be indexed as $LiMn_{0.4}Fe_{0.6}PO_4$ orthorhombic phase. These results further confirm the successful synthesis of crystallized $LiMn_{0.4}Fe_{0.6}PO_4$ coated with amorphous carbon.

The active voltage range of the cathode material (T-400) as valuated by CV is shown in Fig. 5. There are two pairs of redox peaks: peaks A and B centered around 3.5 V corresponding to the redox process of Fe^{3}/Fe^{2+}, and peaks C and D centered around 4.0 V corresponding to the redox process of Mn^{3+}/Mn^{2+}. When the sweep rate is 0.1 mV/s, the difference between the anodic and cathodic peaks' potential $\triangle E_p$ is 0.45 V for Fe^{2+}/Fe^{3+} and 0.4 V for Mn^{2+}/Mn^{3+}. The literature[27] reports that the potential separation between the anodic and cathodic current peaks is 0.39 V for $LiFePO_4$ and 0.5 V for $LiMnPO_4$. Substitution of Fe^{2+} by Mn^{2+} causes a little increase of the potential separation of Fe peaks and a great decrease of Mn peaks. Padli, *et al*[31] explained this phenomenon on a basis of a super-exchange interaction between Fe–O–Mn ions. As the sweep rate is increased to 0.2 mV/s, the intensity and the potential separation of Fe peaks and Mn peaks become greater at the first cycling, which is in agreement with the results of Hashambhoy[28]. CV curves on repeated cycling indicate almost no change for the redox voltage or current with cycling, which indicates that the Fe and Mn oxidation/reduction processes in T-400 are reversible and they can obtain high reversible capacity.

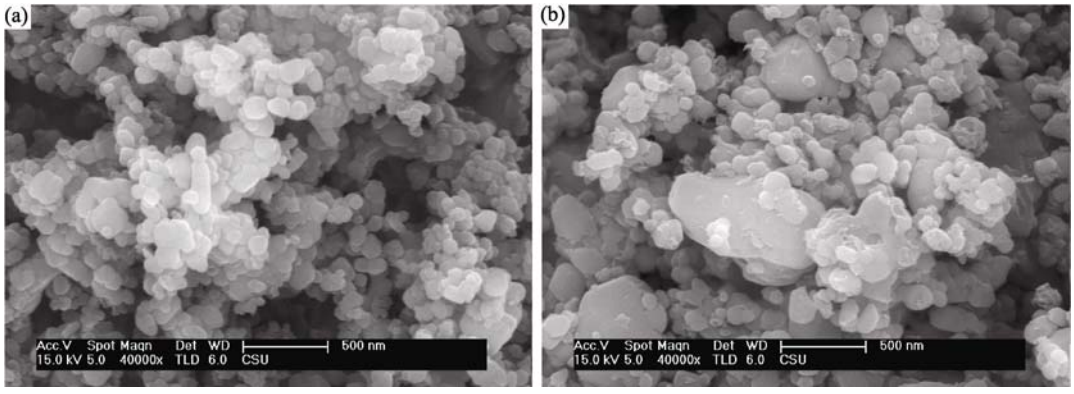

Fig. 3　SEM images of T-400 (the solid-state reaction temperature is 400 ℃) (a) and T-500 (the solid-state reaction temperature is 500 ℃) $LiMn_{0.4}Fe_{0.6}PO_4$/C (b)

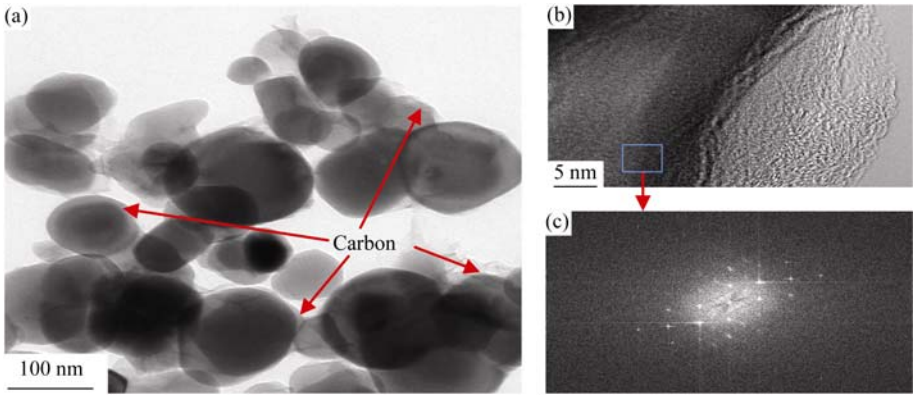

Fig. 4 TEM image (a), high-resolution TEM image (b) and the selected area electron diffraction (SAED) pattern (c) of T-400

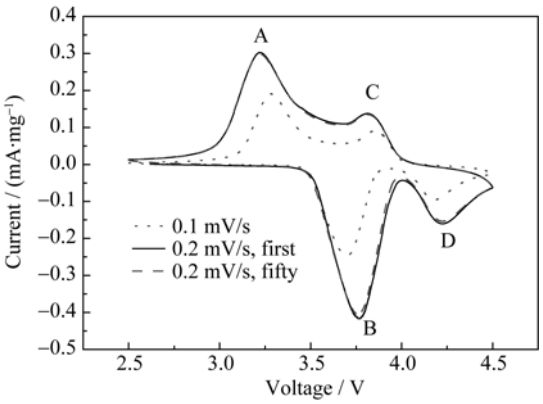

Fig. 5 Cyclic voltammogram curves of T-400

To test the electrochemical performance of the prepared $LiMn_{0.4}Fe_{0.6}PO_4/C$, coin cells using a $LiMn_{0.4}Fe_{0.6}PO_4/C$ cathode and lithium anode are charged and discharged between 2.5 V and 4.5 V. Figure 6 displays the initial charge/discharge voltage profiles of the $LiMn_{0.4}Fe_{0.6}PO_4/C$ synthesized by the new route discussed in this paper. The charging curve shows two distinct plateaus at ~ 3.5 and ~ 4.0 V, which is corresponding to the extraction of lithium ions from $LiMn_{0.4}Fe_{0.6}PO_4$ at these voltage regions for Fe^{3+}/Fe^{2+} and Mn^{3+}/Mn^{2+} couples, respectively. Similarly, the discharge curve shows two corresponding voltage plateaus at ~3.4 and ~3.9 V. At 0.1*C*, an initial discharge capacity of 160 and 155 mAh/g are obtained for T-400 and T-500, respectively, which are close to the theoretical capacity of 170 mAh/g. As the current is increased to 0.5*C*, the initial discharge capacity falls into 143 and 132 mAh/g. These results indicate that the $LiMn_{0.4}Fe_{0.6}PO_4/C$ prepared by the new route discussed in this paper exhibits a good charge and discharge properties. This is ascribed to the smaller particle size allowing rapid diffusion of Li ions.

Figure 7 depicts the excellent cycle performance of $LiMn_{0.4}Fe_{0.6}PO_4/C$ at 0.5*C* rate which was tested over 50 cycles. As can be seen for T-400, although the discharge capacity monotonously decreases from 143 to 132 mAh/g during the first 10 cycles, it then fluctuates between 130 and 138 mAh/g during the successive cycles, and for T-500, the same phenomenon also exists, although the discharge capacity is a little lower. These results demonstrate the well cycling stability of the $LiMn_{0.4}Fe_{0.6}PO_4/C$ prepared by this new route. The good cycling capabilities of $LiMn_{0.4}Fe_{0.6}PO_4/C$ are attributed to the formation of small, uniform particles with much reduced diffusion length for lithium ions and the efficient conductive carbon coating in the material.

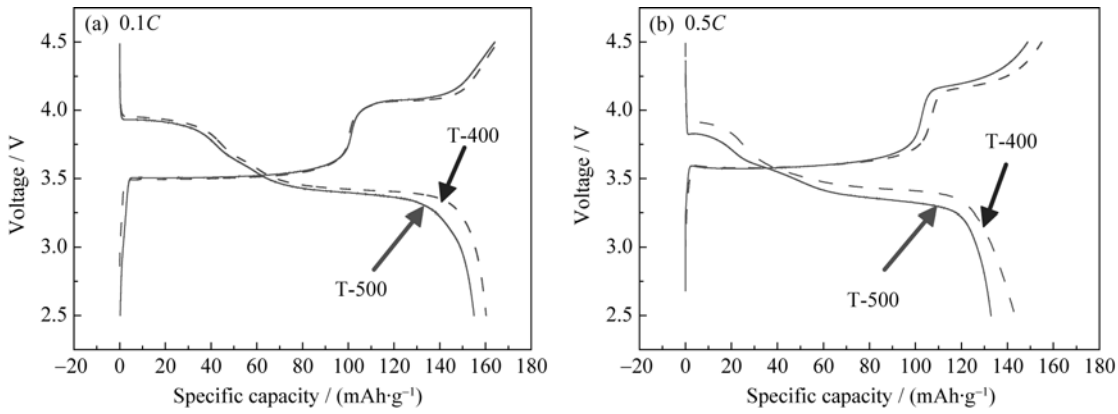

Fig. 6 Charge-discharge curves of lithium cells with T-400 and T-500 as cathode material at 25 ℃

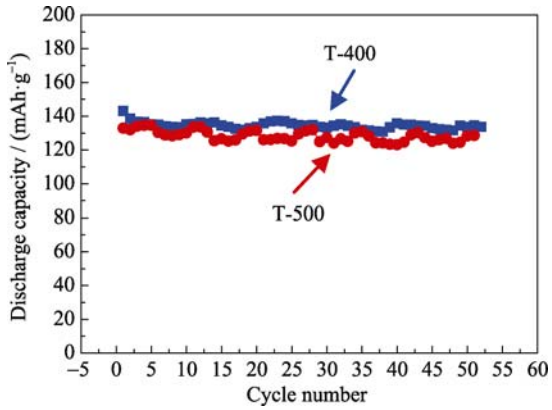

Fig. 7 Cycle performance of lithium cells with T-400 and T-500 as cathode materials at 0.5*C* at 25 ℃

3 Conclusions

Carbon-coated phospho-olivine based on Mn, Fe mixed metals of structural formula $LiMn_{0.4}Fe_{0.6}PO_4$ was synthesized by a new method that combining solid-state reaction with hydrothermal synthesis. The sample T-400 obtained from this method has uniform morphology with the particle size of about 120 nm and a nanometer thick coating of conductive carbon surrounding the particles. The carbon-coated $LiMn_{0.4}Fe_{0.6}PO_4$ composite shows two well-defined redox peaks in 3.3–4.2 V range corresponding to Fe and Mn phases in the sample. On evaluation as the cathode materials in lithium metal battery at room temperature, an initial discharge capacity of 160 mAh/g at 0.1*C*, 143 and 133 mAh/g after 50 cyclies at 0.5*C* is achieved, demonstrating the suitability of the new method for synthesizing the material.

References:

[1] WANG Y G, WANG Y R, HOSONO E, *et al*. The design of a $LiFePO_4$/carbon nano-composite with a core-shell structure and its synthesis by an *in situ* polymerization restriction method. *Angew. Chem. Int. Ed.*, 2008, **47(39):** 7461–7465.

[2] CHOI D, KUMTA P N. Surfactant based Sol-Gel approach to nanostructured $LiFePO_4$ for high rate Li-ion batteries. *J. Power Sources*, 2007, **163(2):** 1064–1069.

[3] CHUNG S Y, BLOKING J T, CHIANG Y M. Electronically conductive phospho-olivines as lithium storage electrodes. *Nat. Mater.*, 2002, **1:** 123–128.

[4] HUANG H, YIN S C, NAZAR L F. Approaching theoretical capacity of $LiFePO_4$ at room temperature at high rates. *Electrochem. Solid-State Lett.*, 2001, **4(10):** A170–A172.

[5] YAMADA A, CHUNG S C, HINOKUMA K. Optimized $LiFePO_4$ for lithium battery cathodes. *J. Electrochem. Soc.*, 2001, **148(3):** A224–A229.

[6] DELACOURT C, POIZOT P, LEVASSEUR S, *et al*. Size effects on carbon-free $LiFePO_4$ powders the key to superior energy density. *Electrochem. Solid-State Lett.*, 2006, **9(7):** A352–A355.

[7] GIBOT P, CASAS-CABANAS M, LAFFONT L, *et al*. Room-temperature single-phase Li insertion/extraction in nanoscale Li_xFePO_4. *Nat. Mater.*, 2008, **7:** 741–747.

[8] MEETHONG N, CARTER W C, CHIANG Y M, *et al*. Size-dependent lithium miscibility gap in nanoscale $Li_{1-x}FePO_4$. *Electrochem. Solid-State Lett.*, 2007, **10(5):** A134–A138.

[9] ZAGHIB K, DONTIGNY M, GUERfi A, *et al*. Safe and fast-charging Li-ion battery with long shelf life for power applications. *J. Power Sources*, 2011, **196:** 3949–3954.

[10] YAMADA A, KUDO Y, LIU K Y. Reaction mechanism of the olivine-type $Li_x(Mn_{0.6}Fe_{0.4})PO_4$ ($0 < x < 1$). *J. Electrochem. Soc.*, 2001, **148(7):** A747–A754.

[11] LI G H, AZUMA H, TOHDA M. Optimized $LiMn_yFe_{1-y}PO_4$ as the cathode for lithium batteries. *J. Electrochem. Soc.*, 2002, **149(6):** A743–A747.

[12] DELACOURT C, LAFFONT L, BOUCHET R, *et al*. Toward understanding of electrical limitations (electronic, ionic) in $LiMPO_4$ (M = Fe, Mn) electrode materials. *J. Electrochem. Soc.*, 2002, **149(5):** A743–A747.

[13] CHOI D, WANG D H, BAE I T, *et al*. $LiMnPO_4$ nanoplate grown via solid-state reaction in molten hydrocarbon for Li-ion battery cathode. *Nano Lett.*, 2010, **10(8):** 2799–2805.

[14] DREZEN T, KWON N H, BOWEN P, *et al*. Effect of particle size on $LiMnPO_4$ cathodes. *J. Power Sources*, 2007, **174(2):** 949–953.

[15] YONEMURA M, YAMADA A, TAKEI Y, *et al*. Comparative kinetic study of olivine Li_xMPO_4 (M=Fe, Mn). *J. Electrochem. Soc.*, 2004, **151(9):** A1352–A1356.

[16] YAMADA A, KUDO Y, LIU K Y. Phase diagram of $Li_x(Mn_yFe_{1-y})PO_4$ ($0 < x, y < 1$). *J. Electrochem. Soc.*, 2001, **148(10):** 1153–1158.

[17] MI C H, ZHANG X G, ZHAO X B, *et al*. Synthesis and performance of $LiMn_{0.6}Fe_{0.4}PO_4$/nano-carbonwebs composite cathode. *Materials Science and Engineering B*, 2006, **129:** 8–13.

[18] SHIN Y J, KIM J K, CHERUVALLY G, *et al*. $Li(Mn_{0.4}Fe_{0.6})PO_4$ cathode active material: Synthesis and electrochemical performance evaluation. *J. Phys. Chem. Solids*, 2008, **69(5/6):** 1253–1256.

[19] KOPE¢ M, YAMADA A, KOBAYASHI G, *et al*. Structural and magnetic properties of $Li_x(Mn_yFe_{1-y})PO_4$ electrode materials for Li-ion batteries. *J. Power Sources*, 2009, **189:** 1154–1163.

[20] LEE K T, LEE K S. Electrochemical properties of $LiFe_{0.9}Mn_{0.1}$

PO_4/Fe_2P cathode material by mechanical alloying. *J. Power Sources*, 2009, **189(1):** 435–439.

[21] BAEK D H, KIM J K, SHIN Y J, *et al*. Effect of firing temperature on the electrochemical performance of $LiMn_{0.4}Fe_{0.6}PO_4$/C materials prepared by mechanical activation. *J. Power Sources*, 2009, **189(1):** 59–65.

[22] NAM K W, YOON W S, ZAGHIB K, *et al*. The phase transition behaviors of $Li_{1-x}Mn_{0.5}Fe_{0.5}PO_4$ during lithium extraction studied by *in situ* X-ray absorption and diffraction techniques. *Electrochem. Commun.*, 2009, **11(10):** 2023–2026.

[23] YAO J, BEWLAY S, KONSTANTIONV K, *et al*. Characterisation of olivine-type $LiMn_xFe_{1-x}PO_4$ cathode materials. *J. Alloys Compd.*, 2006, **425(1/2):** 362–366.

[24] KOSOVA N V, DEVYATKINA E T, SLOBODYUK A B, *et al*. Submicron $LiFe_{1-y}Mn_yPO_4$ solid solutions prepared by mechano-chemically assisted carbothermal reduction: The structure and properties. *Electrochimica Acta*, 2012, **59:** 404–411.

[25] HONMA T, NAGAMINE K, KOMATSU T. Fabrication of olivine-type $LiMn_xFe_{1-x}PO_4$ crystals *via* the glass-ceramic route and their lithium ion battery performance. *Ceramics International*, 2010, **36(3):** 1137–1141.

[26] MOLENDA J, OJCZYK W, MARZEC J. Electrical conductivity and reaction with lithium of $LiFe_{1-y}Mn_yPO_4$ olivine-type cathode materials. *J. Power Sources*, 2007, **174(2):** 689–694.

[27] MOLENDA J, OJCZYK W, ŚWIERCZEK K, *et al*. Diffusional mechanism of deintercalation in $LiFe_{1-y}Mn_yPO_4$ cathode material. *Solid State Ionics*, 2006, **177(26-32):** 2617–2624.

[28] HASHAMBHOY A M, WHITACRE J F. Li diffusivity and phase change in $LiFe_{0.5}Mn_{0.5}PO_4$: A comparative study using galvanostatic intermittent titrationand cyclic voltammetry. *J. Electrochem. Soc.*, 2011, **158(4):** A390–A395.

[29] WANG D, LI H, WANG Z X, *et al*. New solid-state synthesis routine and mechanism for $LiFePO_4$ using LiF as lithium precursor. *J. Solid State Chem.*, 2004, **177(12):** 4582–4587.

[30] PROSINI P P, CAREWSKA M, SCACCIA S, *et al*. Long-term cyclability of nanostructured $LiFePO_4$. *Electrochimica Acta*, 2003, **48(28):** 4205–4211.

[31] PADHI A K, NANJUNDASWAMY K S, GOODENOUGH J B. Phospho-olivines as positive-electrode materials for rechargeable lithium batteries. *J. Electrochem. Soc.*, 1997, **144(4):** 1188–1194.

用固相和水热结合法制备 $LiMn_{0.4}Fe_{0.6}PO_4$/C 复合材料

李 荐[1,2,3], 姚书恒[1], 周宏明[1,2,3], 耿文俊[1]

(1. 中南大学 材料科学与工程学院, 长沙 410083; 2. 湖南省正源储能材料与器件研究所, 长沙 410083; 3. 中南大学 有色金属材料科学与工程教育部重点实验室, 长沙 410083)

摘 要: 以 Li_2CO_3、$FeC_2O_4{\cdot}2H_2O$、$MnCO_3$ 和 $NH_4H_2PO_4$ 为原料, 按 5:6:4:10 的摩尔比混合, 采用固相反应和水热法结合的新方法制备得到 $LiMn_{0.4}Fe_{0.6}PO_4$。通过 XRD、SEM、TEM 以及循环伏安(CV)和充放电测试对材料进行结构、形貌以及电化学性能表征。结果表明, 此方法合成的产物具有单一的橄榄石晶体结构, 颗粒尺寸约为 120 nm, 且表面均匀包覆一层无定形碳。电化学测试结果表明, 样品的循环伏安曲线中有两对氧化还原峰, 分别对应 Fe^{3+}/Fe^{2+}(3.5 V)和 Mn^{3+}/Mn^{2+}(4.0 V)。$LiMn_{0.4}Fe_{0.6}PO_4$/C 在 0.1*C* 下的初始放电比容量为 160 mAh/g, 0.5*C* 下的初始放电比容量为 143 mAh/g, 且具有较好的循环性能。

关 键 词: 锂离子电池; 固相反应; 水热合成; 电化学性能; 电子显微技术

中图分类号: TQ174 **文献标识码:** A